Journal of
Marine Science and Engineering

MDPI

Article

Computational Analysis of an Ammonia Combustion System for Future Two-Stroke Low-Speed Marine Engines

Jose R. Serrano [1], Ricardo Novella [1], Héctor Climent [1], Francisco José Arnau [1], Alejandro Calvo [2,*] and Lauge Thorsen [2]

[1] CMT-Clean Mobility & Thermofluids, Universitat Politècnica de València, 6D-UPV, Camí de Vera, S/N, 46022 Valencia, Spain; jrserran@mot.upv.es (J.R.S.); rinoro@mot.upv.es (R.N.); hcliment@mot.upv.es (H.C.); farnau@mot.upv.es (F.J.A.)

[2] Wärtsilä Services Switzerland Ltd., Schlossmühlestrasse 9, 8500 Frauenfeld, Switzerland; lauge.thorsen@wartsila.com

* Correspondence: alejandro.oliveira@wartsila.com

Abstract: Ammonia, being 17.6% hydrogen by mass, is regarded as a hydrogen carrier and carbon-free fuel as long as its production methods rely on renewable energy sources. The production and combustion of green ammonia do not generate carbon dioxide, offering a promising avenue for substantial reductions in greenhouse gas (GHG) emissions from a well-to-wake perspective. This paper presents a comprehensive methodology for the development and validation of a thermodynamic model for a two-stroke low-speed marine engine incorporating a hybrid ammonia-diesel diffusion combustion system. The simulation tools are rigorously validated using experimental data obtained during diesel operation. Subsequently, the study explores various aspects of the novel ammonia-diesel combustion system, addressing combustion and emissions characteristics. The investigation incorporates diverse simulation scenarios involving direct fuel injection through dedicated valves into the cylinder head of a six-cylinder, turbocharged compression-ignition engine. The engine features two diesel injection valves, employed to initiate the combustion process, and two ammonia injection valves. Simulation scenarios include variations in the injection timing of the pilot diesel injector and the relative orientation of diesel and ammonia sprays. Case C emerges as the preferred configuration, demonstrating superior metrics in terms of combustion stability, air-fuel mixing, and emissions profile compared to other cases. The results indicate a reduction of CO_2 emissions of approximately 95% in mass compared to the baseline diesel operation. Furthermore, notable reductions in NO_x emissions are observed, preliminarily attributed to the lower flame temperature of ammonia. Despite the appearance of N_2O emissions as a result of ammonia oxidation, the overall potential reduction in GHG emissions, in CO_2-equivalent terms, exceeds 85% at selected operating points. This work contributes valuable insights into the optimization of cleaner propulsion systems for maritime applications, facilitating the industry's transition toward more sustainable and environmentally friendly practices.

Keywords: ammonia combustion system; diffusion combustion; two-stroke marine engines; computational model; greenhouse gas emissions

Academic Editor: Decheng Wan

Received: 9 December 2024
Revised: 24 December 2024
Accepted: 26 December 2024
Published: 30 December 2024

Citation: Serrano, J.R.; Novella, R.; Climent, H.; Arnau, F.J.; Calvo, A.; Thorsen, L. Computational Analysis of an Ammonia Combustion System for Future Two-Stroke Low-Speed Marine Engines. *J. Mar. Sci. Eng.* **2025**, *13*, 39. https://doi.org/10.3390/jmse13010039

1. Introduction

Maritime shipping is a key component of the global economy, representing 80–90% of international trade [1]. It is one of the most energy-efficient modes of transport and produces one of the lowest levels of emissions per transport work, but given its sheer scale, the environmental footprint of shipping results in a measurable ecological impact [2].

The European Commission estimates that the maritime sector, with around 1076 million tons of annual carbon dioxide emissions, is responsible for 2.9% of the global anthropogenic GHG emissions [3]. Pursuant to the Paris Climate Agreement and collective efforts to limit the global average temperature rise to +1.5 °C, compared to pre-industrial levels, the International Maritime Organization (IMO) released a set of mandatory measures to reduce GHG emissions from international shipping.

The IMO's updated strategy on reduction in GHG emissions from ships [4], released in July 2023, targets the decline of the carbon intensity of international shipping as an average across international shipping, by at least 40% by 2030, compared to 2008. Additionally, the IMO promotes the uptake of zero or near-zero GHG emission technologies, fuels, and/or energy sources to represent at least 5% of the energy used by international shipping by 2030.

Short-term measures aiming at improving a ship's overall efficiency, such as those adopted in MEPC 76 with the introduction of the so-called Energy Efficiency Existing Ships Index (EEXI), the Carbon Intensity Indicator (CII), and the Ship Energy Efficiency Management Plan (SEEMP) [5] are key in the decarbonization roadmap but insufficient to achieve the GHG emissions reduction outlined by the IMO.

To address the ecological footprint of shipping, a pioneering direct injection ammonia-diesel diffusion combustion system was developed specifically for two-stroke marine engines. This innovative combustion system seamlessly integrates with existing engine components, such as the cylinder head, liners, and injection system of the original diesel engine. As a result, this technology minimizes downtime and capital expenditures for ship owners while significantly reducing greenhouse gas (GHG) emissions. Additionally, the novel design of the combustion system stands out for its flexibility, allowing the ammonia contribution in the combustion process to be adjusted according to the vessel's operational needs. To date, no prior work has achieved such advancements in this domain, marking a significant breakthrough in marine engine retrofit technology.

The use of carbon-free fuels, such as hydrogen and anhydrous ammonia, as fuel for cargo vessels, has been perceived by many as a promising opportunity to enable a pathway toward decarbonizing the maritime industry. Ammonia produced from renewable sources offers many advantages over other maritime fuels, including an established global logistics infrastructure, relatively high energy density, simplicity of storage, and the absence of carbon in its composition, making it a viable avenue to decouple the maritime industry from carbon-based fuels [6].

Research into ammonia's application in the maritime industry has gained momentum in recent years. Works from Thomas Buckley Imhoff et al. [7] provide a theoretical and holistic view on the implementation of an ammonia powertrain in a number of merchant and naval vessels equipped with internal combustion engines and gas turbines.

Numerical studies [8,9] conducted on dual-fuel engines employing an ammonia-diesel premixed combustion system indicate significant reductions in greenhouse gas (GHG) emissions can be attained with sustained high Ammonia Energy Ratios (AERs). However, nitrogen oxide emissions tend to increase with higher AERs, as indicated in various numerical investigations [10,11]. Long Liu et al. assess the viability of utilizing ammonia in low-speed marine engines, comparing low-pressure and high-pressure fuel admission methods. Their findings emphasize the favorable emissions profile associated with the high-pressure fuel admission mode.

Xinran Wang et al. [12] and Aaron J. Reiter et al. [13,14] retrofitted a 4-cylinder in-line 4-stroke engine with a low-pressure gaseous ammonia fuel injection system and analyzed the combustion and emissions characteristics of a CI engine with varying AERs and the diesel pilot injection timing. Their investigations show a reduction in NO_x and GHG emissions with AERs in the vicinity of 50%, with higher ammonia shares negatively impacting engine stability and exhaust gas emissions.

In a separate study, Yoichi Niki et al. [15] investigated the emissions and combustion characteristics of a premixed ammonia-diesel dual-fuel combustion in a single-cylinder diesel engine, finding that higher AERs reduce CO_2 and CO emissions, whereas NO_x, ammonia and N_2O emissions followed the opposing pattern. Other studies [16], validated against experimental data, explored low-pressure fuel intake systems for mixtures of natural gas and ammonia, highlighting a monotonous reduction in CO_2 emissions, though with adverse effects on NO_x and unburned fuel with increased ammonia fuel shares.

Yasuhisa Ichikawa et al. [17] presented a novel three-layer stratified fuel injection concept for two-stroke marine engines in which liquid ammonia is sequentially injected between two layers of high-reactivity fuel. The experimental study suggests that such an injection strategy, when optimized, could substantially reduce N_2O emissions compared to more conventional fuel injection strategies, ultimately mitigating the GHG impact of ammonia-diesel engines compared to traditional diesel engines.

At the time of writing, very limited experimental studies delving into the direct injection phenomenon and diffusion combustion of ammonia in engine-like conditions have been published. Yanzhi Zhang et al. [18] conducted a numerical investigation of high-pressure direct ammonia injection and its spray characteristics under GDI and diesel-like engine conditions. Their study evaluated various vaporization models within the Lagrangian particle tracking (LPT) framework, demonstrating their ability to appropriately replicate liquid ammonia spray characteristics under non-flash boiling conditions. Zhenxian Zhang et al. [19] and Jiangping Tian et al. [20] performed detailed studies on the diesel-ammonia diffusion combustion modes in a constant-volume combustion vessel and a Rapid Compression and Expansion Machine (RCEM), respectively. Their investigations reveal the importance of the spray interaction between the pilot diesel and the ammonia jets in sustaining ammonia diffusion combustion and delve into the impact of other injection parameters on the combustion process.

Recent developments in the maritime industry highlight the growing interest in ammonia as a sustainable future fuel. The European Maritime Safety Agency [21] conducted a comprehensive study that delves into the sustainability, availability, techno-economic analysis, safety, and environmental aspects of using ammonia as fuel in shipping. Additionally, environmental assessments, including the potential impact of large ammonia spills at sea, have been addressed in reports by organizations like the Environmental Defense Fund [22].

Given ammonia's potential significance in the future of the maritime sector and the ambitious targets outlined in the IMO decarbonization strategy, endeavors to incorporate green ammonia as a fuel for two-stroke engines, currently the primary propulsion system in the shipping sector, are in progress. This work introduces a methodology employed to design an ammonia-diesel diffusion combustion system tailored for in-service two-stroke marine engines and a number of case studies aiming at identifying the relevance of certain critical parameters in such an endeavor.

2. Materials and Methods

This section provides an overview of the methodologies and tools employed in the initial design of a direct injection ammonia-diesel diffusion combustion system, developed as retrofit technology for two-stroke marine engines in service. The approach stands out for its seamless integration of fluid-dynamic and combustion simulation tools, which enable an existing diesel engine—requiring minimal modifications and retaining its critical components—to be readily adapted for ammonia. This strategy ensures that upgrades to the simulation tools are minimal and underscores the low retrofitting effort required to implement this innovative ammonia-diesel combustion system on existing marine engines.

The initial design of the ammonia-diesel combustion system was carried out primarily with two simulation tools: Virtual Engine Model (VEMOD), a 0D–1D gas-dynamics simulation tool, and CONVERGE Studio 3.0, a 3D Computational Fluid Dynamics (CFD) tool. Effectively combining these tools is essential for the establishment of a robust design strategy and is of utmost importance in developing a comprehensive virtual model of the engine. More information on the tools is available in references [23,24].

To ensure robust predictability of the simulation tools used in the ammonia-diesel studies, a rigorous validation process was conducted. This phase aimed to verify the capability of the simulation tools to accurately predict the internal phenomena occurring within the engine with an appropriate degree of precision. For this purpose, experimental data from the diesel combustion system currently implemented in the laboratory engine under study was used, ensuring a faithful reproduction of the engine's behavior during the scavenging and combustion processes. Following the validation phase, the tools were employed in a series of prospective studies with the objective of enhancing the comprehension of the novel combustion system under different operating conditions. The outcome of these is presented in the Results and Discussion section.

This methodology was selected as the most appropriate approach, given that no experimental data currently exists for this novel ammonia-diesel combustion system. This approach is widely recognized as standard practice in the development of novel combustion technologies and has been successfully used in other scientific studies, such as that of Qian et al. [8]. In their work, a computational fluid dynamics (CFD) model was coupled with an ammonia/n-dodecane combustion mechanism to investigate the impact of combustion control parameters in the performance of marine engines. Similarly, other research works, including those by Yin et al. [25], Lu et al. [26], and Zhu et al. [27], employ comparable methodologies, combining CFD models with combustion mechanisms from the literature, and report their usefulness in predicting the behavior of ammonia combustion systems.

2.1. Validation of the Simulation Models

A 0D–1D virtual engine model was created using VEMOD, featuring the integration of all engine cylinders with the corresponding air management system. This model enables a comprehensive assessment of overall engine performance, in-cylinder parameters, and turbocharger operation.

In the initial stage of validation, the 0D–1D virtual engine model was correlated with experimental data, with specific attention directed toward the two fundamental phases within a two-stroke engine cycle: the gas exchange and combustion stages.

Following the successful validation of the 0D–1D virtual engine model, a detailed 3D representation of a single cylinder was generated to provide a more profound understanding of the combustion process. Having reached a satisfactory level of confidence in the resemblance between the 0D–1D virtual engine model and the physical engine following the preceding validation exercise, certain outputs from the 0D–1D virtual engine model simulations were employed as boundary conditions for the 3D virtual cylinder model. Subsequently, the model underwent meticulous validation against both experimental data and the 0D–1D virtual engine model.

The three-dimensional cylinder model was developed to analyze the gas flow and thermodynamic phenomena within the cylinder over a complete engine revolution using CONVERGE® v3.0.21. The modeling process was divided into two phases: the scavenging phase, capturing gas flow characteristics from the Exhaust Valve Opening (EVO) to the Exhaust Valve Closing (EVC) angles, and the combustion phase, covering the inverse cycle from EVC to EVO. Key events in the latter phase included the end of the compression stroke, fuel injection, combustion, and the start of the expansion stroke.

To ensure a balance between computational efficiency and accuracy, an optimization exercise determined that a base mesh size of 20 mm was optimal. This resolution maintained sufficient detail while avoiding excessive computational costs. Embedding strategies and Adaptive Mesh Refinement (AMR) techniques were employed to improve resolution in regions of interest and during critical events such as Intake Port Opening (IPO) and Closing (IPC), Exhaust Valve Opening (EVO), and Closing (EVC), and the fuel injection process.

The spray dynamics within the cylinder were modeled using a Discrete Droplet Model (DDM), which represented sprays as collections of discrete droplets, modeled as Lagrangian particles. The Kelvin-Helmholtz (KH) and Rayleigh-Taylor (RT) models were used to simulate the primary atomization and breakup of liquid fuel jets into droplets. Droplet collisions and coalescence were captured using the No Time Counter (NTC) and O'Rourke models, while wall-film and O'Rourke models simulated droplet interactions with solid surfaces, including splashing, film formation, and evaporation.

The experimental data for this research was taken from a Wärtsilä six-cylinder RT-Flex50DF engine. The engine has a cylinder bore of 500 mm and a stroke of 2050 mm. Under the chosen operating conditions, the engine yields a nominal power output of 7.950 kW at 115.5 rpm, with a BMEP of 17.1 bar (Table 1).

Table 1. Engine metadata 6RT-Flex50DF for diesel operation, general technical data for the WinGD 2-Stroke Engine [28].

Parameter	Value
Nº of cylinders	6
Cylinder bore	500 mm
Piston stroke	2050 mm
Nominal speed	115.5 rpm
Nominal Mean effective pressure	17.1 bar
Geometrical compression ratio	17.0
Stroke/bore	4.1
Nominal power	7950 kW

2.1.1. Gas Exchange

Figure 1 shows the results of the gas exchange validation of the 0D–1D and 3D simulation models where the data have been normalized to preserve its confidentiality.

For this exercise, the 3D cylinder model was initialized at the crank angle corresponding to the EVO with the values provided by the 0D–1D engine model.

Figure 1a,c shows a comparison between the 0D–1D and 3D simulation models of the intake and exhaust mass flow rate and the trapped mass in one cylinder, where positive values indicate flow entering the cylinder. The green and yellow stripes indicate the opening and closing angles of the intake ports and the exhaust valve. Despite the lack of test data, a consistent behavior of both simulation tools is visible in these representations. Figure 1b,d–f shows a satisfactory correlation between simulation models and the experimental data. Figure 1b shows a slight deviation in the cylinder pressure of the 0D–1D engine model compared to the test data and the 3D cylinder model, which is believed to stem from small geometrical discrepancies that generate acoustic disturbances, affecting the pressure waves during the scavenging phase. Figure 1d displays the intake instantaneous pressure and the average temperature on the intake boundary of the cylinder, where a good correlation between simulations and experiments is visible. Figure 1e shows the exhaust average pressure and temperature in the exhaust boundary of the cylinder, indicating a pronounced difference in the temperature profiles preliminarily attributed to a limited deviation in heat transfer between the exhaust gas and the surrounding manifold and air. However, the lack of instantaneous temperature test data for this parameter complicates the formulation of suitable conclusions. Figure 1f shows the exhaust valve lift profile, where the 3D cylinder model and the test data are perfectly aligned, whereas VEMOD's valve lift profile has been approximated using breakpoints for simplicity.

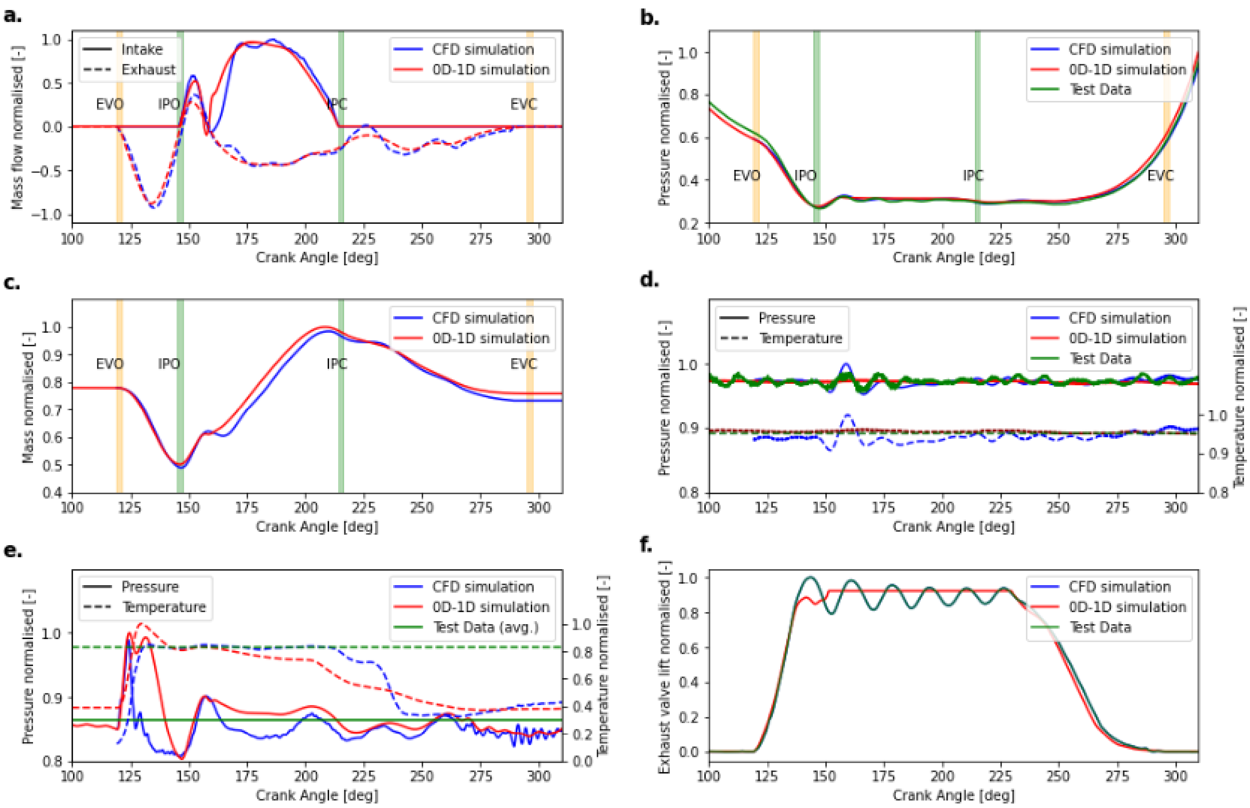

Figure 1. Normalized engine parameters characteristic of the gas exchange phase at nominal engine operating conditions compared between CFD, VEMOD, and test data, where available. (**a**) Intake and exhaust mass flow comparison. (**b**) Cylinder pressure comparison. (**c**) Cylinder mass comparison. (**d**) Intake pressure and temperature. (**e**) Exhaust pressure and temperature. (**f**) Exhaust valve lift.

2.1.2. Combustion

A reduced chemical mechanism from B. Wang et al. [29] consisting of 495 reactions and 74 species was embedded into the 3D cylinder model and dictates the combustion process in both, the purely diesel and the ammonia-diesel simulation cases.

The reduced mechanism was validated against experimental ignition delay times (IDTs) for operating conditions representative of a diffusion combustion process (Figures 2 and 3). The ignition delay time predictions were made by using a homogeneous batch reactor of constant volume with Cantera 2.6 [30]. In general, a good agreement between the reduced model and the experimental data are achieved.

Figure 4 depicts the normalized cylinder pressure and heat release rate operating with diesel at the nominal conditions for both the simulation models and experimental data.

A so-called Heat Release Law, extracted from the experimental heat release rate, is used as input to the 0D–1D engine model, whereas the 3D cylinder model employs the reduced chemical-kinetic mechanism from B. Wang et al. [29], by means of direct integration methods, to simulate the combustion process. It is visible that both simulation models capture the combustion process satisfactorily, although some differences in the heat release rates and cylinder pressures are observable. The 0D–1D engine model renders a lower firing pressure than its counterparties despite producing the highest peak heat release rate. A plausible explanation for this is that an overestimated heat transfer during the compression stroke results in a lower compression pressure as the fresh air gives away too much heat as the piston moves from BDC to TDC (i.e., the compression process is less adiabatic), which in turns, generates a lower compression pressure, and therefore, a lower peak firing pressure. The 3D cylinder model yields a heat release rate and cylinder pressure that match closely with those from the experimental data. Only minor differences emerge in the later stage of the combustion process, highlighting subtle discrepancies in the tail-end combustion compared to the experimental data.

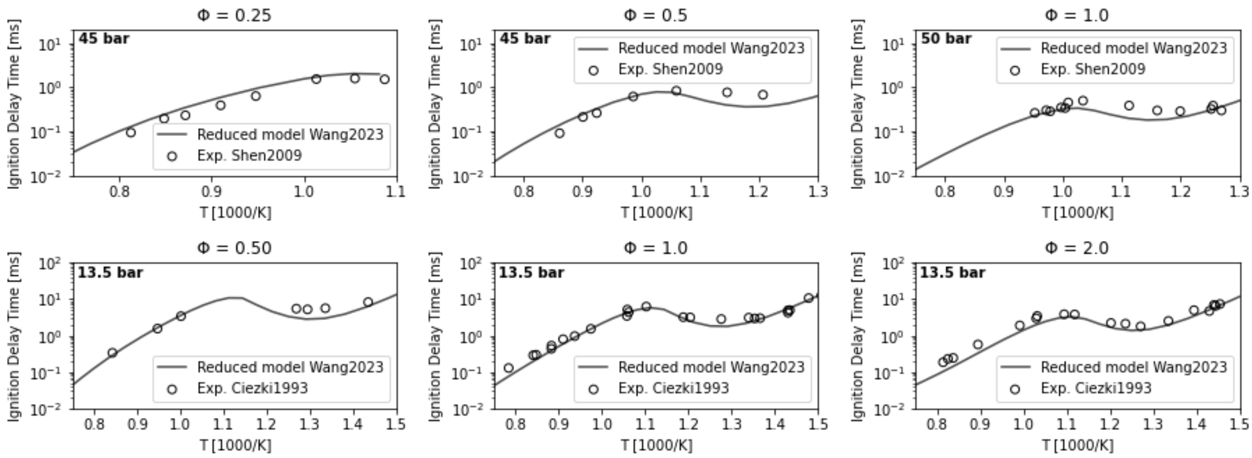

Figure 2. Ignition delay times of an n-heptane-air mixture at different pressures and equivalence ratios. Comparison between the selected reduced kinetic mechanism from Wang et al. 2023 [29] and empirical data from shock tube experiments [31,32].

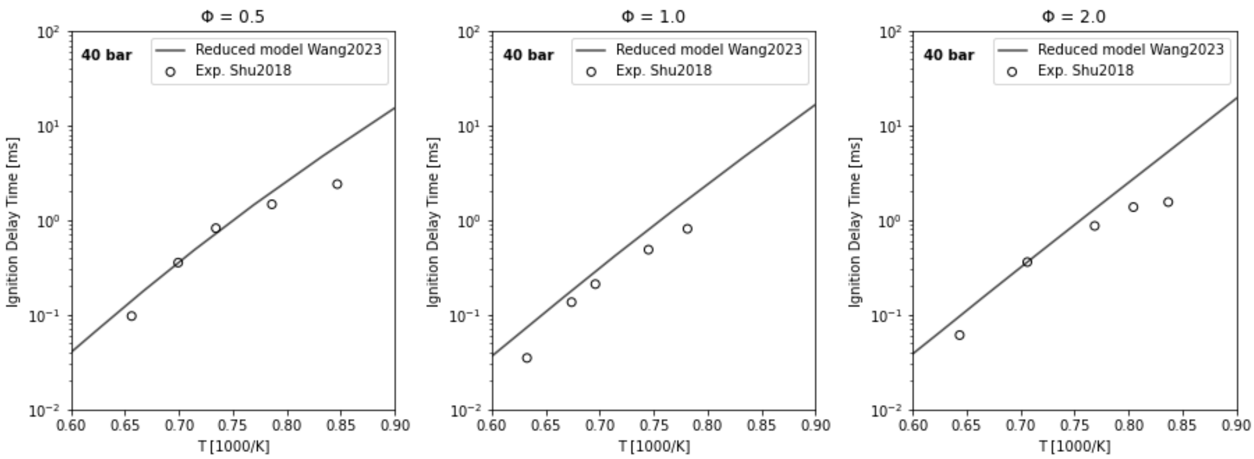

Figure 3. Ignition delay times of an ammonia-air mixture at 40 bar at different equivalence ratios. Comparison between the selected reduced kinetic mechanism from Wang et al. 2023 [29] and empirical data from shock tube experiments [33].

The resemblance between the outputs of the simulation tools and the existing test data for the Wärtsilä 6RT-Flex50DF engine running with diesel leads the authors to conclude that the simulation tools have been effectively validated for this specific engine configuration and instills confidence in their suitability for the forthcoming prospective investigations to offer guidance for the initial design of an ammonia-diesel combustion system.

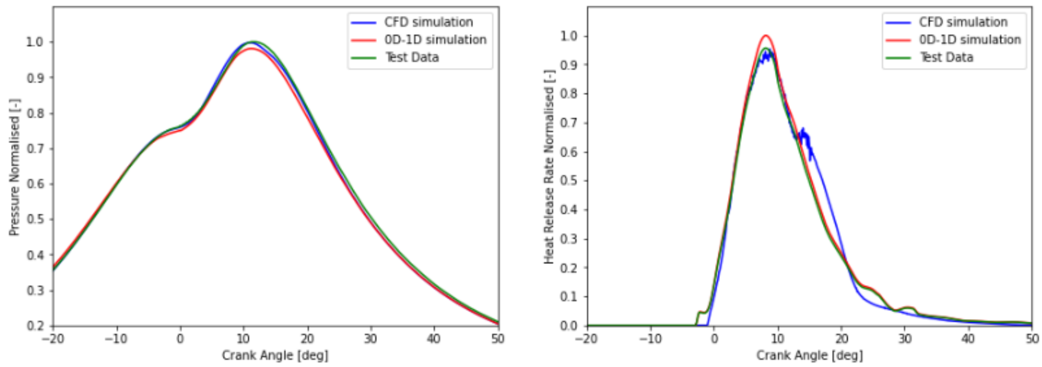

Figure 4. Normalized cylinder pressure and heat release rate operating with diesel at nominal engine conditions CONVERGE vs. VEMOD vs. experimental data. Left: cylinder pressure. Right: heat release rate.

2.2. Setup of the Ammonia-Diesel Simulation Tools

The engine configuration(s) for which the ammonia-diesel prospective studies were performed are described in Table 2. In this occasion, a reduced nominal engine power output and speed were targeted to avoid excessively large fuel quantities, given the reduced LHV of ammonia compared to diesel. By doing this, the ammonia injection valves would not need to undergo extensive modifications to provide the necessary fuel amount.

Table 2. Engine metadata 6RT-Flex50DF for ammonia operation, general technical data for WinGD 2-Stroke Engine [28].

Parameter	Value
N° of cylinders	6
Cylinder bore	500 mm
Piston stroke	2050 mm
Nominal speed	99 rpm
Nominal Mean effective pressure	14.4 bar
Geometrical compression ratio	17.0
Stroke/bore	4.1
Nominal power	5730 kW

The two additional ammonia injection valves were modeled as depicted in Figure 5 on the cylinder cover, at a given distance from the diesel injection valves, which serve the purpose of initiating the combustion of ammonia and are, hereinafter, referred to as pilot injection valves.

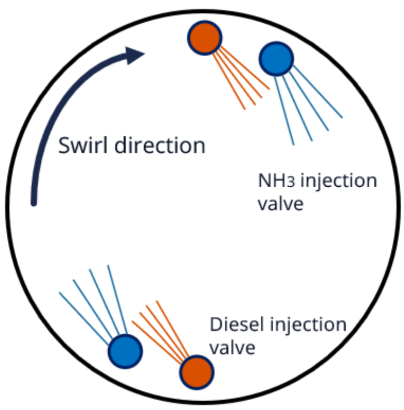

Figure 5. Sketch of the combustion chamber with the diesel and ammonia injection valves and the swirl motion, top view.

This combustion system is characterized by two pairs of injection valves symmetrically arranged in the cylinder head, by means of which a high-reactivity fuel ignites a low-reactivity fuel through controlled collisions of their independent jets. The system strategically uses swirl motion to ensure an optimal interaction between the diesel and ammonia jets. The meticulous design of the combustion system ensures high combustion efficiency with ammonia as the primary fuel, which, combined with its ease of implementation, makes this technology uniquely suitable for retrofitting marine engines.

3. Results and Discussion

A series of prospective studies were conducted employing simulation tools validated with experimental data from the 6RT-Flex50DF engine. Initially, a cold-flow simulation was carried out to characterize the scavenging cycle under nominal engine operating conditions. The cold-flow simulation was performed during the open-loop phase, spanning from the Exhaust Valve Opening (EVO) angle to the Exhaust Valve Closing (EVC) angle. Subsequently, the cylinder conditions at EVC were employed as initial conditions for the combustion simulation, extending from the crank angle corresponding to EVC to EVO, thus completing the engine cycle.

3.1. Gas Exchange

Figure 6 presents key metrics for understanding the gas exchange phase in two-stroke engines. Vertical yellow stripes indicate the crank angles at which the exhaust valve opens and closes, while green stripes indicate the opening and closing of the intake ports.

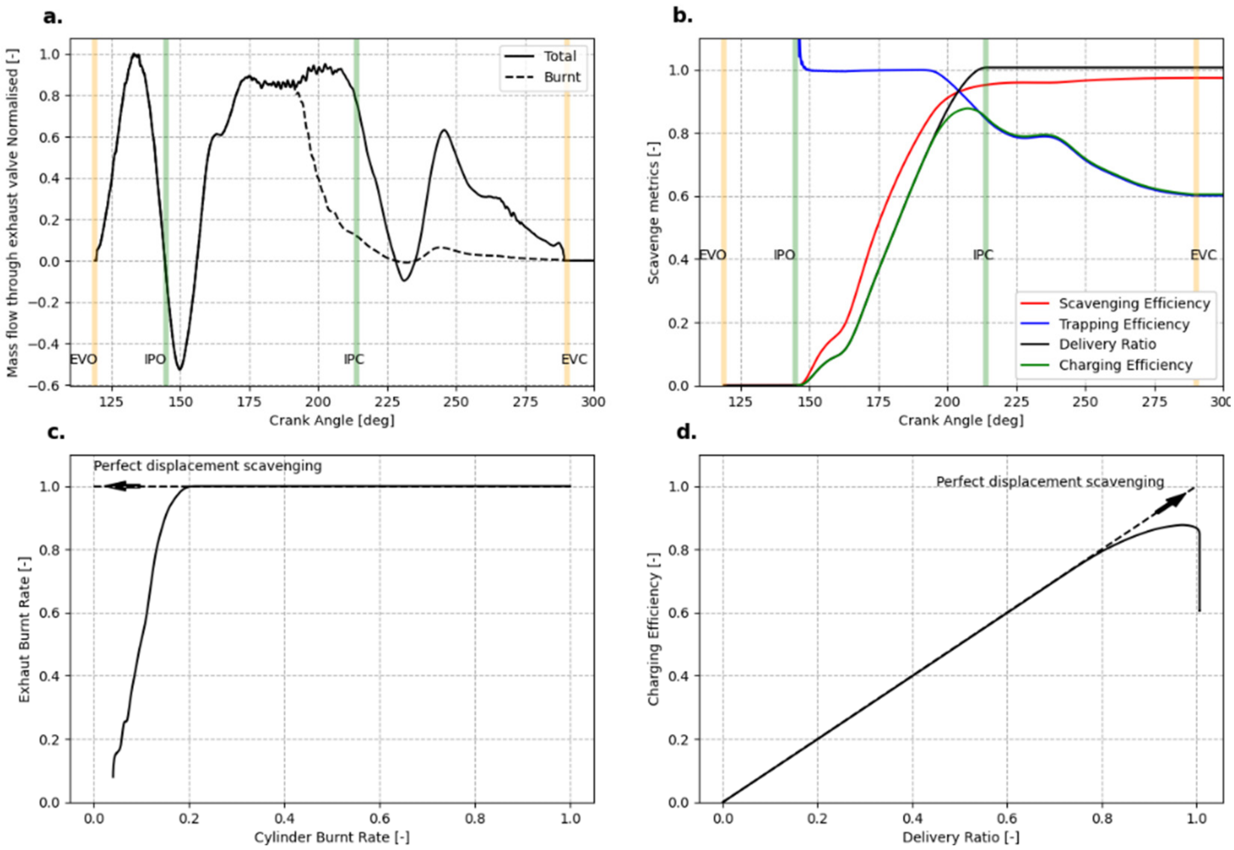

Figure 6. Normalized engine parameters characteristic of the gas exchange process at nominal engine operating conditions. (**a**) Gas mass flow through the exhaust valve. (**b**) Scavenging metrics. (**c**) Exhaust Burnt Rate vs. Cylinder Burnt Rate. (**d**) Charge Efficiency vs. Delivery Ratio.

Figure 6a depicts the normalized exhaust mass flow rate during the scavenging phase. It includes the burnt mass flow rate, representing residual gasses from the previous combustion cycle, and the total mass flow rate, accounting for all gasses leaving the cylinder during the scavenging loop. The difference between total and burnt mass flow represents the mass of fresh air short-circuited during the scavenging phase.

Figure 6b presents fundamental metrics crucial for understanding the efficiency of the gas exchange process. Scavenging Efficiency (SE), defined as the ratio of air mass trapped in the cylinder to the total trapped mass, approaches values near 98% at the end of the scavenging process. Uniflow-scavenging two-stroke engines exhibit high scavenging efficiencies compared to crossflow and loop-scavenging engines [34].

Trapping Efficiency (TE), defined as the ratio of trapped air mass to the total air mass flowing through the cylinder during scavenging, is lower than SE due to the substantial amount of short-circuited air, a characteristic feature of two-stroke marine engines. The main purpose of the short-circuited air is to serve as a cooling medium for the cylinder components, mitigating excessive heat generated during the combustion event.

Delivery Ratio (DR) represents the amount of air flowing through the cylinder with respect to a theoretical maximum cylinder capacity, denoted as the reference mass. As depicted in Figure 6b, the engine investigated exhibits a DR surpassing unity, indicating that the volume of fresh air traversing the cylinder is sufficient to replenish the entire cylinder with air at the reference conditions. These elevated DR values align with the characteristics typically observed in slow-turning engines featuring large Specific Time Area (STA) values.

Charging Efficiency (CE) determines the trapped air mass relative to the reference mass, indicating how effectively the cylinder traps fresh air during the gas exchange phase.

Figure 6c provides insight into the evolution of residual gasses in the cylinder as the scavenging process progresses. As the Cylinder Burnt Rate (CBR) moves from right to left, the Exhaust Burnt Rate (EBR) values equal to unity indicate a perfect displacement of the residual gasses by fresh air. In this case, a rapid drop of EBR is visible beyond CBR ≈ 0.2, signifying that a stratified flow is established, which negatively impacts the evacuation of residual gasses and allows fresh air to bypass the cylinder.

Figure 6d delineates the progression of fresh air bypassing the cylinder throughout the gas exchange phase. In this specific engine, Charging Efficiency (CE) levels off when the Delivery Ratio (DR) exceeds 0.8, indicating the initiation of air bypass, detrimentally affecting Charging Efficiency. Following the closure of the intake ports, a notable reduction in CE is evident. This decline is attributed to the fraction of air that circulates through the exhaust valve after the intake port closure, reducing the mass of air in the cylinder at EVC.

In uniflow scavenging two-stroke engines, the primary source of air turbulence arises from the swirl motion. To characterize this turbulence within the cylinder, the magnitude of the air velocity vector under different planes, at two distinct crank angles, is depicted in Figure 7. The top illustration captures the air motion in the cylinder at EVC, while the bottom figure renders the same parameter prior to the fuel injection event.

The representations reveal that the air velocity at the central region of the cylinder is nearly zero, exhibiting an unequivocal increase in magnitude toward the periphery of the piston. Moreover, the air velocity at the periphery diminishes as the piston advances linearly toward the Top Dead Center (TDC). This reduction is primarily attributed to air friction with the static cylinder liner during the compression stroke.

As the piston approaches the Top Dead Center (TDC), the decrease in cylinder volume results in a more uniform distribution of air velocity along the edge of the piston, which contributes to an enhanced homogeneity in the swirl motion prior to the combustion phase.

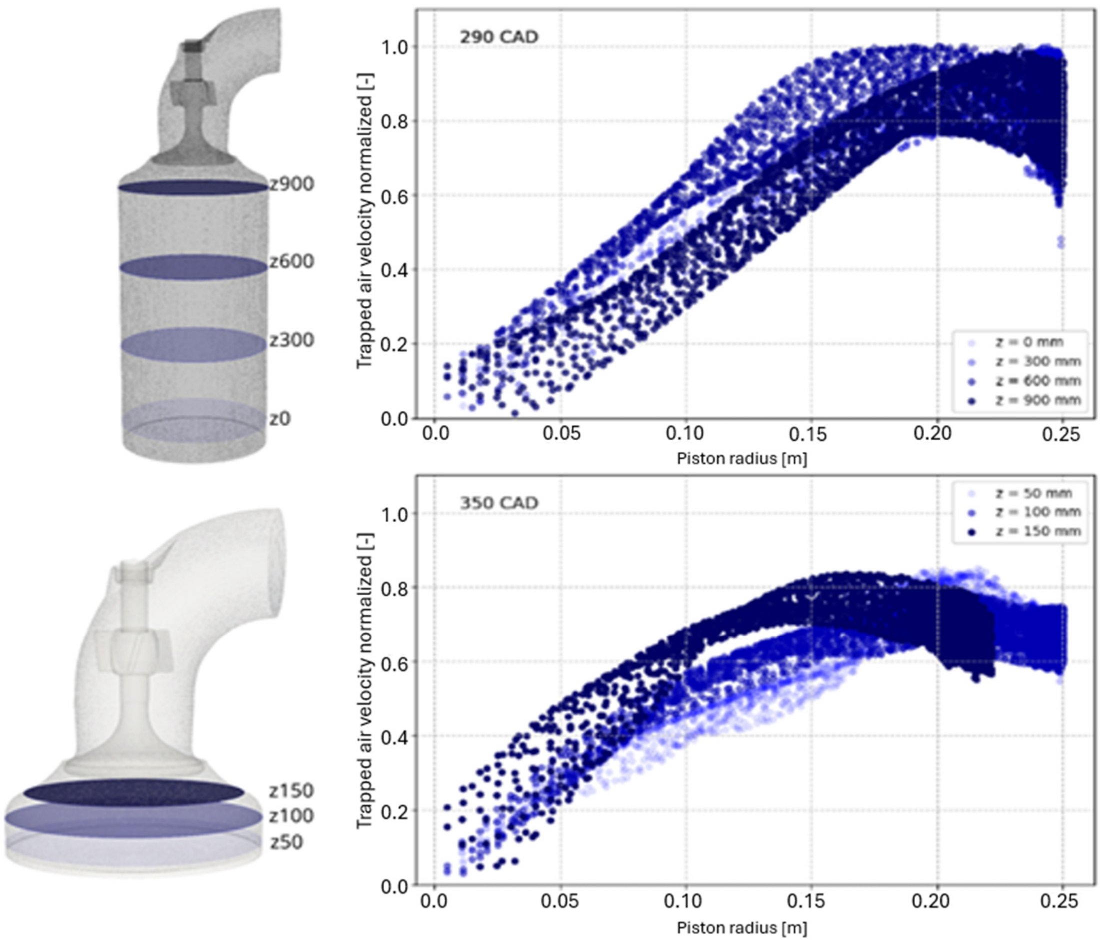

Figure 7. Normalized in-cylinder air velocity distribution in the radial direction at different heights. Top: 290 CAD. Bottom: 350 CAD.

3.2. Combustion

In the formulation of the combustion system, the influence of two critical factors were assessed: the pilot diesel injection timing, and the spray orientation of the ammonia injection valves. This evaluation was conducted under the engine operating conditions outlined in Table 2. Moreover, it became necessary to establish the Ammonia Energy Rate (AER), which is defined as the proportion of the ammonia fuel energy in relation to the total fuel energy injected into the cylinder. In our investigation, a 95% AER was employed. A 5% Diesel Energy Rate (DER) was necessary to initiate the combustion of ammonia.

Table 3 summarizes the simulated cases presented in this section, without detailing the reference injection timing and spray configurations.

Table 3. Summary of combustion simulations.

Simulation Case	Ammonia Energy Ratio (AER, [%])	Start of Injection (SOI) Ammonia	Start of Injection (SOI) Diesel	Ammonia Spray Orientation	Diesel Spray Orientation
A	95	θ_A	θ_D—3.5 CAD	Spray Configuration 1	Spray Configuration 1
B	95	θ_A	θ_D—5.5 CAD	Spray Configuration 1	Spray Configuration 1
C	95	θ_A	θ_D—3.5 CAD	Spray Configuration 2	Spray Configuration 1
D	0	N/A	θ_D	N/A	Spray Configuration 2

The baseline diesel combustion case denoted as Case D, with a 0% ammonia substitution, is incorporated into certain plots to elucidate the distinctions between a pure diesel and a hybrid ammonia-diesel combustion system.

3.2.1. Injection Timing of Diesel Pilot

Two distinct scenarios were examined concerning the injection timing of the pilot diesel injection: Case A, with the pilot diesel injection timing set 3.5 CAD earlier than that of the baseline diesel start of injection (θ_D), and the reference ammonia injection timing (θ_A), and Case B, where the pilot diesel injection was advanced 2 CAD with respect to Case A, thereby lengthening the dwell time between the pilot and the main injections.

The combustion process in both cases is illustrated in Figure 8, with Case A on the top and Case B on the bottom. A Φ-T chart and visualizations of the fuel sprays and flames in the combustion chamber elucidate key events of the combustion process.

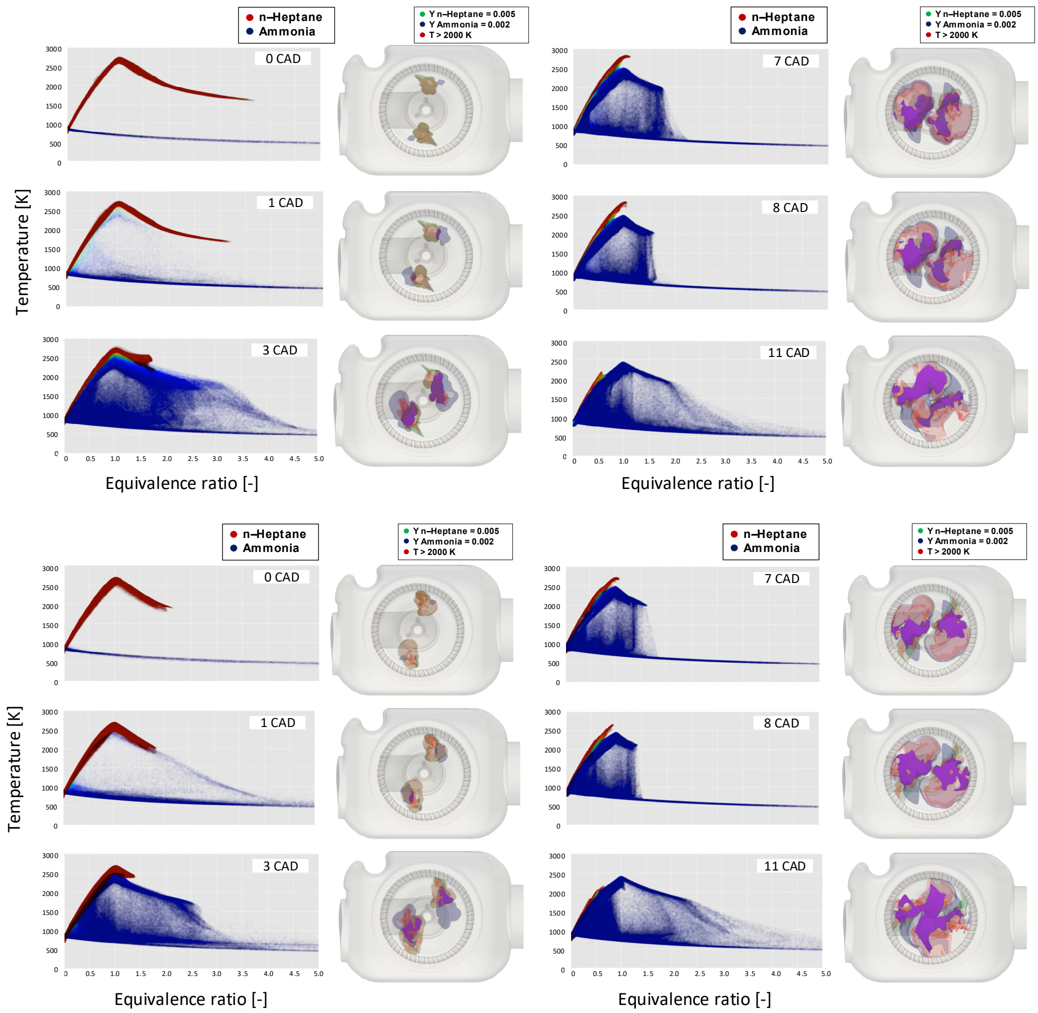

Figure 8. CFD simulation of an ammonia-diesel combustion with a 95% ammonia energy share showing the Φ-T diagram and cylinder combustion visualization at different crank angles. Top: Case A. Bottom: Case B.

Analyzing the initial moment at t = 0 CAD, it is evident that the pilot fuel, injected via the two pilot injectors, undergoes combustion in both cases. Case A presents a wider Φ range under which n-heptane burns, attributed to the later initiation of the pilot diesel injection compared to Case B.

Subsequent instants reveal the interaction between the pilot flame and the ammonia jet, injected from the ammonia injection valves. The Φ-T chart indicates that a portion of the ammonia present in the chamber ignites due to the high local temperatures produced by the pilot flame. The mass of ammonia that ignites first is likely closest to the pilot flame. The ignition process of ammonia is comparable in both cases, leading to the conclusion that advancing the pilot diesel injection does not substantially affect the start of ammonia combustion.

At t = 3 CAD, the diffusion combustion of ammonia is established. In this instant, the contact volume between n-heptane and ammonia, depicted in the combustion chamber in purple, is the smallest in Case B. This can be discerned in the Φ-T chart by the lower values of Φ under which ammonia burns, and may be attributed to the diesel pilot flame nearing extinguishment when the ammonia flame enters full diffusion combustion.

In subsequent instants, a forward movement of the ammonia flame's lift-off length is observed in the cut view of the combustion chamber, and occurs equally in Cases A and B. This signifies that the diffusion ammonia flame is unable to self-sustain under the prevailing chamber conditions. Despite continuous fuel injection, the combustion rate decays, presumably concluding with the extinction of the flame a short time after. This effect is evident in the Φ-T chart as the ammonia under reacting conditions retracts to Φ values below 1.7. It is likely that the low local temperatures in the vicinity of the injection valve, caused by the large latent heat of evaporation of the injected ammonia, is the main reason for the increase in the flame lift-off length, resulting in a cloud of unburned ammonia coexisting near the nozzle tip.

The swirling motion plays a key role towards the final phase of the combustion. In this stage, the ammonia flames on one side of the cylinder advance toward the opposing ammonia injection valves, where they interact with the unburned mass of ammonia and provide the activation energy needed for ignition. This effect is clearly visible in Figure 9a where a double peak in the Heat Release Rate due to the sudden combustion of ammonia is present.

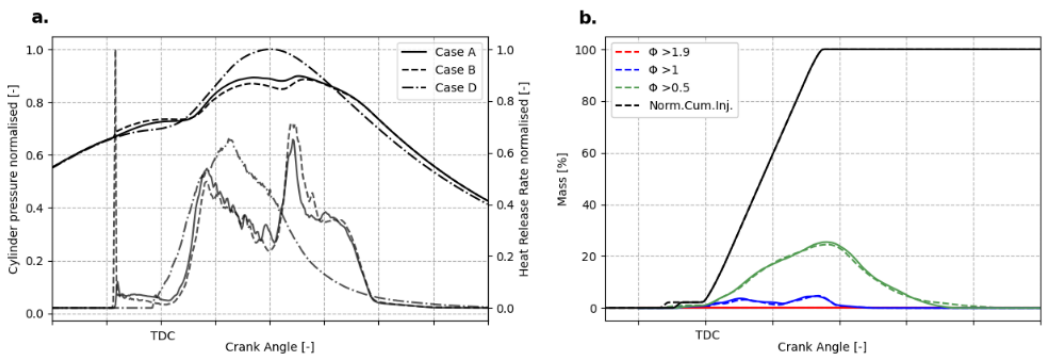

Figure 9. (**a**) Cylinder pressure and Heat Release Rate comparison between Case A, Case B, and Case D. (**b**) Mixture mass distribution at different equivalence ratios for Case A and Case B.

A corresponding double peak is also observed in the cylinder pressure, with Case B exhibiting a somewhat lower pressure than Case A, attributed to a slightly reduced interaction of the pilot diesel flame with the ammonia jet at the time of ammonia ignition.

While the reignition phenomenon positively contributes to completing the combustion, it cannot be relied upon universally since variations in engine operating conditions, such as reduced swirl motion and fuel quantity, are likely to diminish or eliminate these benefits, increasing the risk of significant ammonia slip at the end of combustion.

Figure 9a underscores the significance of the pilot injection timing on the combustion of the pilot flame. The early injection of n-heptane results in a longer ignition delay of the jet, inducing a larger portion of the fuel to undergo sudden premixed combustion. This aspect is supported by Figure 10a, wherein Case B momentarily exhibits a higher mass of unburned n-heptane than Case A, owing to the longer ignition delay of the pilot diesel jet with the earlier injection start.

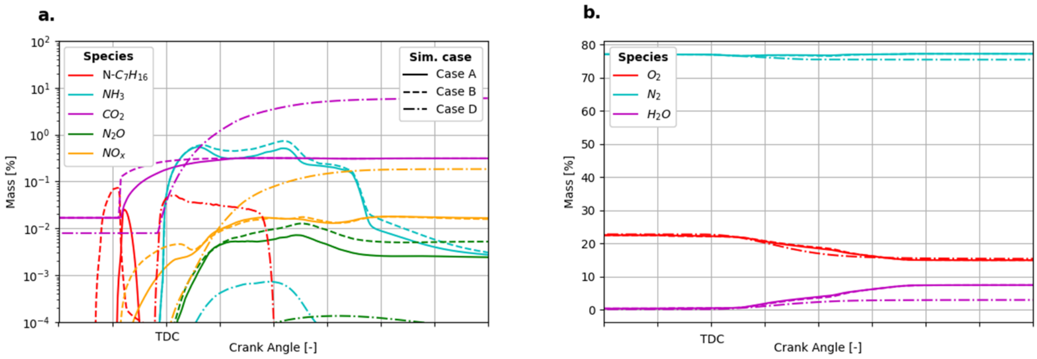

Figure 10. (**a**) Evolution of pollutant species during the combustion process for Case A, Case B, and Case D. (**b**) Evolution of O_2, N_2, and H_2O during the combustion process for Case A, Case B, and Case D.

Case D renders a discernible reduction in premixed peak in comparison to cases A and B, aligning with its later start of the diesel injection. Despite achieving comparable peak heat release rates (HRR) across all three cases, Case D shows a higher peak cylinder pressure attributed to a larger heat release in the proximity of the top dead center (TDC). Noteworthy is the visibly shorter tail combustion duration of ammonia in contrast to diesel, a phenomenon that holds the potential for enhancing the combustion performance of the former by facilitating a more centralized combustion around TDC.

Figure 9b illustrates the mixture mass evolution over various equivalence ratios throughout the combustion phase, indicating changes in the air/fuel mixing process in the combustion chamber. This metric is useful in tracking the mixture of hydrogen and carbon atoms with the oxygen available, disregarding the dissociation of the fuel molecules due to oxidation. Notably, both cases show minimal fuel in very rich regions ($\Phi > 1.9$), with most of it concentrated in the range $\Phi > 0.5$. This observation suggests that the mixing processes in both cases are remarkably similar.

Figure 10 depicts the evolution of various gas species during the combustion process. N-heptane and ammonia correspond to the pilot and main fuels in cases A and B, respectively. A comparison of the mass of ammonia in the cylinder reveals that the advancement of the pilot injection timing has a limited but non-negligible impact on ammonia combustion. This influence is consistent with the double-peak pattern observed in Figures 8 and 9 and is also evident in the evolution of the ammonia mass in the cylinder.

The substantial reduction in ammonia mass to values near zero signifies the completion of combustion with minimal ammonia slip. Notably, the emissions of nitrous oxide, a potent greenhouse gas, are significantly higher in Case B, which highlights the role that the interaction between pilot and main injection plays in the formation of pollutant species.

The carbon dioxide (CO_2) emission levels are consistent between Cases A and B, both significantly reduced by an order of magnitude when contrasted with Case D. This underscores the substantial reduction in greenhouse gas emissions attainable through the incorporation of ammonia in the combustion process of two-stroke low-speed engines. Similarly, the levels of nitrogen oxides (NO_x) emissions are markedly lower in the ammonia-diesel diffusion combustion. This reduction can be ascribed to the lower combustion temperatures resulting from ammonia combustion, thereby decreasing the thermal NO_x production. Nevertheless, the pathways governing NO_x production in ammonia combustion are intricate, and a meticulous evaluation is essential to discern the specific contribution of thermal and fuel-derived NO_x in the overall NO_x emissions.

When comparing the indicated efficiency of Cases A, B, and D, the simulations using ammonia as the primary fuel achieve up to 0.6% higher efficiency compared to those using dodecane. This improvement is attributed to the higher heat capacity ratio of the resulting species from ammonia combustion. The increased nitrogen (N_2) concentration in the species present during the expansion stroke, resulting from ammonia combustion, contributes to this effect, as N_2 has a higher heat capacity ratio than carbon dioxide (CO_2), which is produced during dodecane combustion. The combustion patterns obtained in Case A and Case B are almost identical, resulting in very similar indicated efficiencies for both cases.

3.2.2. Fuel Jets Orientation

The preceding analysis provided insights that suggested the necessity for enhanced interaction between the diesel pilot flame and the ammonia jets to address the suboptimal initial combustion of ammonia and the subsequent reignition effect observed toward the end of the combustion phase. Consequently, Case C was formulated with a revised spray orientation designed to alleviate these challenges. Figure 11 illustrates, on the top, the baseline simulation case (referred to as Case A) and, on the bottom, the newly configured Case C, where the adjusted jet orientation has been implemented.

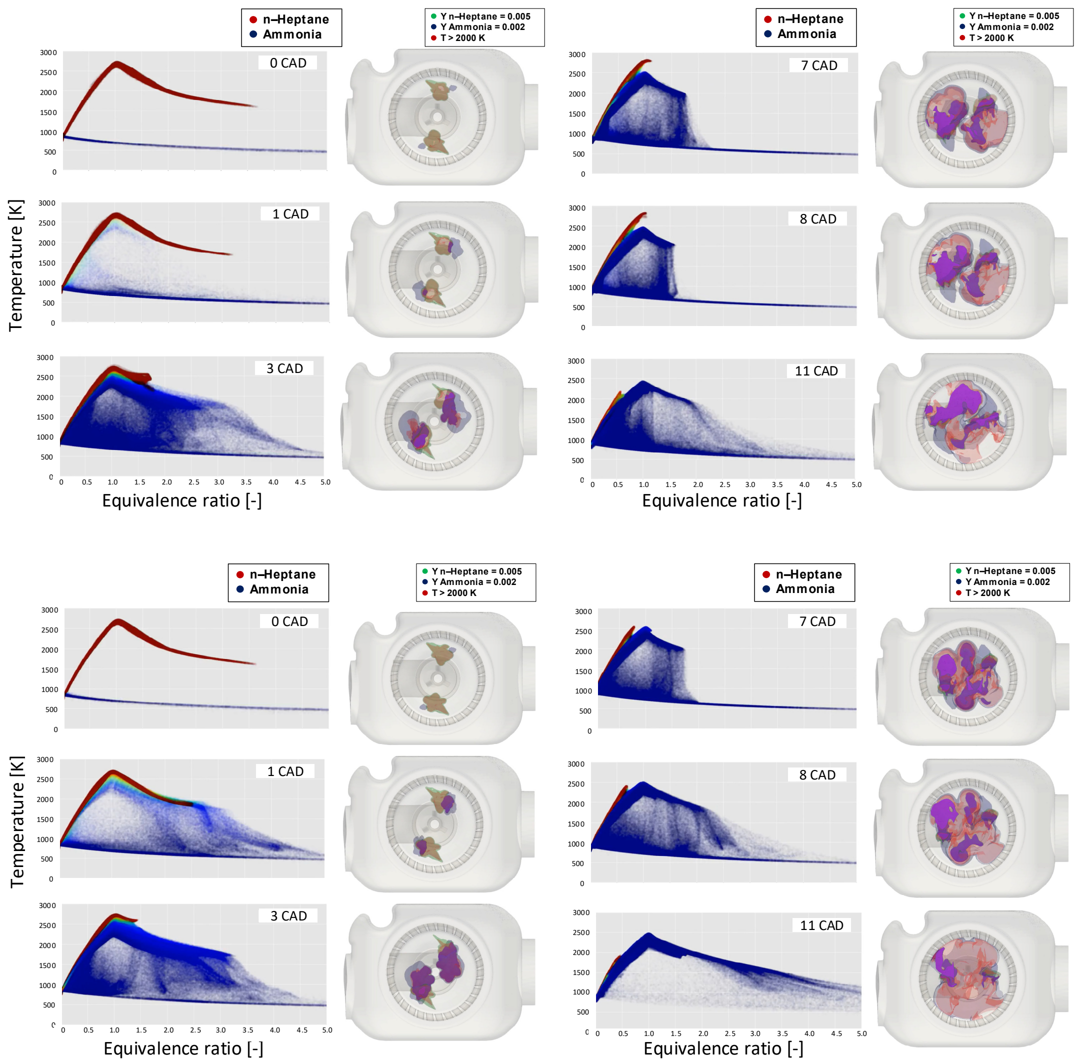

Figure 11. CFD simulation of an ammonia-diesel combustion with a 95% ammonia energy share showing the Φ-T diagram and cylinder combustion visualization at different crank angles. Top: Case A. Bottom: Case C.

The combustion behavior of the diesel pilot injection at t = 0 CAD closely mirrors Case A and Case C, given that the pilot injection timing remains identical in both scenarios.

At t = 1 CAD, it is evident that the combustion strategy employed in Case C results in better initial activation of ammonia, likely attributable to the enhanced interaction between the diesel pilot flame and the ammonia jet.

Subsequently, the following moment reveals a well-established and developed diffusion flame of ammonia. Case C exhibits a markedly larger interaction volume between n-heptane and ammonia, indicating a pronounced improvement compared to Case A. Furthermore, an examination of the Φ-T diagram suggests that ammonia combustion is consistent across a broader Φ range, suggesting a larger mass of ammonia under reactive conditions.

Observing subsequent time points, the lift-off length of the ammonia flame in Case C also appears to progress forward with time, indicating that the diffusion combustion of ammonia cannot be self-sustained under the existing chamber conditions.

From a pragmatic standpoint, the notable reduction in ammonia mass near the nozzle tip in Case C, as compared to Case A, contributes to a diminished reignition phenomenon. This observation is validated by Figure 12, where Case C does not display the double-peak combustion pattern evident in Case A. Furthermore, a distinctly different Heat Release Rate pattern emerges as a consequence of the more optimal spray orientation.

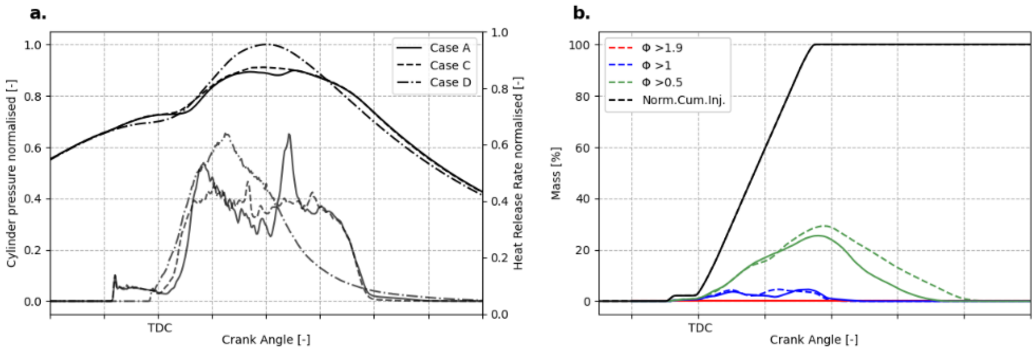

Figure 12. (**a**) Cylinder pressure and Heat Release Rate comparison between Case A, Case C, and Case D. (**b**) Mixture mass distribution at different equivalence ratios for Case A and Case C.

Figure 12a shows that the adjustment of the spray orientation exerts no influence on the combustion process of the pilot injection. This is evident when examining the progression of the Heat Release Rate in the initial moments of combustion. However, a distinct effect is observed in the combustion of ammonia, with Case C demonstrating a more sustained Heat Release Rate throughout the combustion phase, absent of the double-peak pattern visible in Case A. This phenomenon is discernible in the cylinder pressure trace, where Case C exhibits a smoother shape without the characteristic double peak.

A clear influence on the mixing process is evident in Figure 12b, suggesting an improved air/fuel mixing process in Case C as there appears to be more mixture mass under the $\Phi > 0.5$ curve, implying that a larger portion of fuel reached conditions conducive to ignition.

Figure 13 shows a clear improvement in the emissions profile derived from the combustion process from Case C.

The progression of n-heptane mass throughout the combustion phase is consistent in both cases, as is the evolution of CO_2, indicating that the combustion process of the diesel pilot injection is identical.

The instantaneous unburned fuel mass of ammonia is considerably reduced with the new jet orientation, which suggests that, once the diffusion flame of ammonia is established, the fuel undergoes continuous combustion at a slightly faster rate than the injection rate, resulting in less accumulation and, therefore, reducing the formation of rich pockets of fuel.

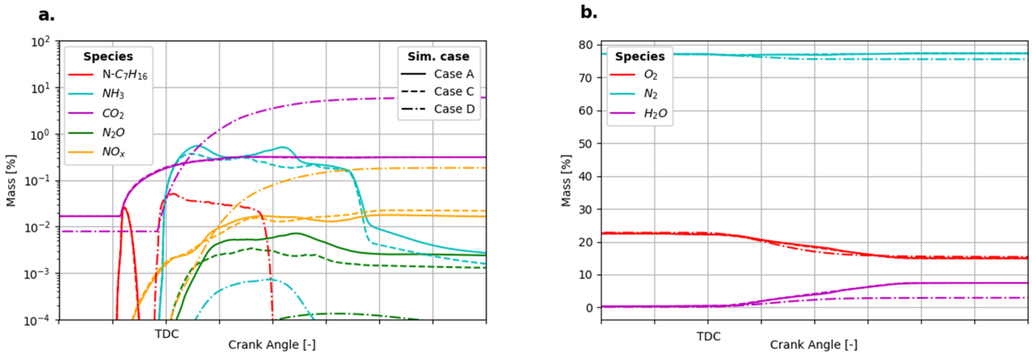

Figure 13. (**a**) Evolution of pollutant species during the combustion process for Case A, Case C, and Case D. (**b**) Evolution of O_2, N_2, and H_2O during the combustion process for Case A, Case C, and Case D.

N_2O emissions are greatly diminished with the enhanced spray orientation. Conversely, there is a modest increase in NO_x emissions observed in case C, potentially attributed to increased local temperatures resulting from the enhanced interaction between the diesel flame and ammonia spray, resulting in higher thermal NO_x production.

Figure 12a reiterates the enhanced emission performance of the ammonia-diesel diffusion combustion system (cases A and C) in comparison to the conventional diesel diffusion combustion mode (Case D) as illustrated in Figure 10a.

When comparing the performance of Cases A, C, and D, Case C demonstrates up to a 1% improvement in indicated efficiency compared to the diesel-only simulation (Case D). This enhancement is primarily attributed to the higher heat capacity ratio of the species resulting from ammonia combustion, combined with a sustained combustion pattern, leading to better overall efficiency. Additionally, Case C achieves approximately 0.4% greater indicated efficiency than Case A, owing to improved combustion characteristics resulting from the optimized spray orientation of the ammonia jet relative to the pilot diesel jet.

This study showcases the viability of using ammonia as a fuel for two-stroke marine engines. Its use in sufficiently large quantities can yield CO_2 reductions of up to 95% in gravimetric terms and an overall GHG reduction exceeding 85% when compared to conventional diesel-fueled two-stroke engines. The optimization of critical parameters, such as the orientation of fuel jets, demonstrates that combustion stability can be achieved satisfactorily. Moreover, the simulation methodology employed in these exercises proves to be robust and functional, confirming its potential for further applications in the design of experimental activities.

4. Conclusions

This study presents a pioneering direct injection ammonia-diesel diffusion combustion system conceived as a retrofit technology for in-service two-stroke marine engines. The foundation of the study is a comprehensive numerical approach that effectively integrates validated simulation tools with experimental data, establishing the necessary framework for the development of a dual-fuel combustion strategy where n-heptane, a surrogate of diesel oil, is employed to initiate the combustion of ammonia within the cylinder. After validation, the simulation tools are employed to assess the impact of the diesel pilot injection timing and the relative spray orientation between the diesel and the ammonia injection valves at the nominal engine operating conditions. The key findings of this research are outlined below:

(1) Ammonia, due to the absence of carbon atoms in its composition, its relatively high energy density, and the established experience in storage and handling, emerges as

a viable alternative to conventional hydrocarbon fuels for shipping. The approach presented allows for the implementation of ammonia as fuel in two-stroke marine engines in service with minimal modification to the baseline diesel engine setup.

(2) The method outlined, which integrates validated numerical models, demonstrates a remarkable alignment between simulation tools and experimental data. It proves highly effective in predesigning a direct injection ammonia-diesel diffusion combustion system tailored for in-service two-stroke marine engines and in assessing the impact of key combustion control parameters.

(3) Within the range explored, the pilot injection timing significantly affects the pilot combustion process due to the varying ignition delay times resulting from advancing the start of the diesel pilot injection. Nevertheless, the diesel pilot injection timing proves to be of limited influence on the ammonia combustion.

(4) Under all simulation conditions, the ammonia lift-off length moves frontwards, primarily due to its low flame speed. The interaction between the diesel pilot spray, and the ammonia spray is identified to be of crucial importance for the success of the combustion system, as it plays a critical role in the reignition of the unburned ammonia in the vicinity of the nozzle tip.

(5) The analysis of different combustion cases demonstrates that the case with improved sprays interplay exhibits a favorable combustion pattern characterized by stability, improved self-sustenance, reduced ammonia slip, diminished Nitrous Oxides (N_2O) formation, and improved air-fuel mixing.

(6) The novel ammonia-diesel diffusion combustion system achieves significant reductions in CO_2 emissions compared to conventional diesel systems. When factoring in the global warming potential (GWP) of nitrous oxide, the overall reduction in greenhouse gas (GHG) emissions exceeds 85%. Furthermore, NO_x emissions are reduced by over 80%, likely due to the lower adiabatic flame temperature of ammonia. However, the high hydrogen content of ammonia results in a substantial increase in water production, which may have detrimental effects on the lifetime of engine components due to increased corrosion.

These findings collectively advance our understanding of key factors influencing the efficiency and environmental impact of the ammonia-diesel diffusion combustion system for two-stroke marine engines. Nevertheless, there are still unexplored areas and unanswered questions related to the pilot injection parameters, spray interplay and combustion chamber conditions that warrant attention in future research endeavors.

Author Contributions: Conceptualization, J.R.S., R.N. and A.C; methodology, J.R.S., R.N., H.C., F.J.A. and A.C.; software, R.N. and F.J.A.; validation, R.N. and L.T.; formal analysis, J.R.S., R.N., H.C., A.C. and L.T.; investigation, R.N., H.C. and F.J.A.; resources, R.N., F.J.A. and L.T.; data curation, R.N., H.C. and A.C.; writing—original draft preparation, A.C; writing—review and editing, J.R.S., R.N., H.C., F.J.A. and L.T.; visualization, R.N., H.C., A.C. and L.T.; supervision, J.R.S., R.N., H.C. and F.J.A.; project administration, J.R.S., R.N. and A.C.; funding acquisition, R.N., A.C. and L.T. All authors have read and agreed to the published version of the manuscript.

Co-funded by the European Union

Funding: Funded by the European Union. Views and opinions expressed are however those of the author(s) only and do not necessarily reflect those of the European Union or

CINEA. Neither the European Union nor the granting authority can be held responsible for them. This work was supported by the Swiss State Secretariat for Education, Research and Innovation (SERI) under contract number 22.00047. The authors want to express their gratitude to CONVERGENT SCIENCE for their kind support by providing access to CONVERGE CFD modeling platform.

Institutional Review Board Statement: Not applicable.

Informed Consent Statement: Not applicable.

Data Availability Statement: Restrictions apply to the availability of these data. Data were obtained from Wärtsilä Services Switzerland Ltd. and are available on request from the corresponding author with the permission of Wärtsilä Services Switzerland Ltd., as the data are the intellectual property of the company.

Acknowledgments: This research was conducted as part of the European-funded Ammonia2-4 project with additional private financial support from Wärtsilä Services Switzerland Ltd. The experimental data for validation purposes were provided by Wärtsilä Services Switzerland Ltd.

Conflicts of Interest: Authors Alejandro Calvo and Lauge Thorsen were employed by the company Wärtsilä Services Switzerland Ltd. The remaining authors declare that the research was conducted in the absence of any commercial or financial relationships that could be construed as a potential conflict of interest.

References

1. Balcombe, P.; Brierley, J.; Lewis, C.; Skatvedt, L.; Speirs, J.; Hawkes, A.; Staffell, I. How to decarbonise international shipping: Options for fuels, technologies and policies. *Energy Convers. Manag.* **2019**, *182*, 72–88. [CrossRef]
2. Lister, J.; Poulsen, R.T.; Ponte, S. Orchestrating transnational environmental governance in maritime shipping. *Glob. Environ. Change* **2015**, *34*, 185–195. [CrossRef]
3. EU. European Commissiong—Reducing Emissions from the Shipping Sector. Available online: https://climate.ec.europa.eu/eu-action/transport-emissions/reducing-emissions-shipping-sector_en (accessed on 17 February 2024).
4. IMO. Annex 1, Resolution MEPC.377(80), 2023. IMO Strategy on Reduction of GHG Emissions from Ships. 2023. Available online: https://www.imo.org/en/OurWork/Environment/Pages/2023-IMO-Strategy-on-Reduction-of-GHG-Emissions-from-Ships.aspx (accessed on 17 February 2024).
5. Psaraftis, H.N. Shipping decarbonization in the aftermath of MEPC 76. *Clean. Logist. Supply Chain* **2021**, *1*, 100008. [CrossRef]
6. Ash, N.; Scarbrough, T. *Sailing on Solar: Could Green Ammonia Decarbonise International Shipping*; Environmental Defense Fund: London, UK, 2019.
7. Imhoff, T.B.; Gkantonas, S.; Mastorakos, E. Analysing the Performance of Ammonia Powertrains in the Marine Environment. *Energies* **2021**, *14*, 7447. [CrossRef]
8. Qian, Y.; Sun, Y.; Gong, Z.; Meng, S.; Wei, X.; Tang, B.; Wan, J. Study on the impact mechanism of ammonia energy fraction on in-cylinder combustion and pollutant generation under wide operation conditions of medium-speed diesel engines. *Fuel* **2024**, *360*, 130617. [CrossRef]
9. Shin, J.; Park, S. Numerical analysis for optimizing combustion strategy in an ammonia-diesel dual-fuel engine. *Energy Convers. Manag.* **2023**, *284*, 116980. [CrossRef]
10. Liu, L.; Wu, Y.; Wang, Y. Numerical investigation on the combustion and emission characteristics of ammonia in a low-speed two-stroke marine engine. *Fuel* **2022**, *314*, 122727. [CrossRef]
11. Liu, L.; Wu, Z.; Tan, F.; Wang, Y. CFD investigation the combustion characteristic of ammonia in low-speed marine engine under different combustion modes. *Fuel* **2023**, *351*, 128906. [CrossRef]
12. Wang, X.; Li, T.; Chen, R.; Li, S.; Kuang, M.; Lv, Y.; Wang, Y.; Rao, H.; Liu, Y.; Lv, X. Exploring the GHG reduction potential of pilot diesel-ignited ammonia engines-Effects of diesel injection timing and ammonia energetic ratio. *Appl. Energy* **2024**, *357*, 122437. [CrossRef]
13. Reiter, A.J.; Kong, S.C. Demonstration of compression-ignition engine combustion using ammonia in reducing greenhouse gas emissions. *Energy Fuels* **2008**, *22*, 2963–2971. [CrossRef]
14. Reiter, A.J.; Kong, S.C. Combustion and emissions characteristics of compression-ignition engine using dual ammonia-diesel fuel. *Fuel* **2011**, *90*, 87–97. [CrossRef]
15. Niki, Y.; Hirata, K.; Kobayashi, K.; Shimizu, Y. Development of Premixed Ammonia Combustion Strategy with Minimum Emissions for Marine Diesel Engines. In Proceedings of the CIMAC Congress, Busan, Republic of Korea, 12–16 June 2023; National Institute of Maritime, Port and Aviation Technology: Tokyo, Japan, 2023.

16. Wei, W.; Li, G.; Zhang, Z.; Long, Y.; Zhang, H.; Huang, Y.; Zhou, M.; Wei, Y. Effects of ammonia addition on the performance and emissions for a spark-ignition marine natural gas engine. *Energy* **2023**, *272*, 127092. [CrossRef]
17. Ichikawa, Y.; Niki, Y.; Takasaki, K.; Kobayashi, H.; Miyanagi, A. NH3 combustion using three-layer stratified fuel injection for a large two-stroke marine engine: Experimental verification of the concept. *Appl. Energy Combust. Sci.* **2022**, *10*, 100071. [CrossRef]
18. Zhang, Y.; Xu, L.; Zhu, Y.; Xu, S.; Bai, X.S. Numerical study on liquid ammonia direct injection spray characteristics under engine-relevant conditions. *Appl. Energy* **2023**, *334*, 120680. [CrossRef]
19. Zhang, Z.; Long, W.; Cui, Z.; Dong, P.; Tian, J.; Tian, H.; Meng, X. Visualization study on the ignition and diffusion combustion process of liquid phase ammonia spray ignited by diesel jet in a constant volume vessel. *Energy Convers. Manag.* **2024**, *299*, 117889. [CrossRef]
20. Tian, J.; Zhang, X.; Cui, Z.; Ye, M.; Wang, Y.; Xu, T.; Dong, P. Visualization study on ammonia/diesel dual direct injection combustion characteristics and interaction between sprays. *Energy Convers. Manag.* **2024**, *299*, 117857. [CrossRef]
21. European Maritime Safety Agency. *Update on Potential of Biofuels in Shipping*; EMSA: Lisbon, Portugal, 2022.
22. Environmental Defense Fund. *Ammonia at Sea: Studying the Potential Impact of Ammonia as a Shipping Fuel on Marine Ecosystems*; Environmental Defense Fund: New York, NY, USA, 2022.
23. Martin, J.; Arnau, F.; Piqueras, P.; Auñon, A. *Development of an Integrated Virtual Engine Model to Simulate New Standard Testing Cycles*; Technical Paper No. 2018-01-1413; SAE International: Warrendale, PA, USA, 2018. [CrossRef]
24. CONVERGE CFD Software. Available online: https://convergecfd.com/products/converge-cfd-software#:~:text=CONVERGE%20is%20a%20leading%20computational,accuracy,%20efficiency,%20and%20innovation (accessed on 17 February 2024).
25. Yin, B.; Lu, Z.; Shi, L.; Lu, T.; Ye, J.; Ma, J.; Wang, T. Numerical simulation of a spark ignition ammonia marine engine for future ship power applications. *Energy* **2024**, *302*, 131823. [CrossRef]
26. Lu, Z.; Ye, J.; Gui, Y.; Lu, T.; Shi, L.; An, Y.; Wang, T. Numerical study of the compression ignition of ammonia in a two-stroke marine engine by using HTCGR strategy. *Energy* **2023**, *276*, 127578. [CrossRef]
27. Zhu, J.; Zhou, D.; Yang, W.; Qian, Y.; Mao, Y.; Lu, X. Investigation on the potential of using carbon-free ammonia in large two-stroke marine engines by dual-fuel combustion strategy. *Energy* **2023**, *263*, 125748. [CrossRef]
28. Win GD General Technical Data (WinGTD). Available online: https://www.wingd.com/en/engines/general-technical-data-(gtd)/ (accessed on 17 February 2024).
29. Wang, B.; Dong, S.; Jiang, Z.; Gao, W.; Wang, Z.; Li, J.; Yang, C.; Wang, Z.; Cheng, X. Development of a reduced chemical mechanism for ammonia/n-heptane blends. *Fuel* **2023**, *338*, 127358. [CrossRef]
30. Goodwin, D.G.; Moffat, H.K.; Schoegl, I.; Speth, R.L.; Weber, B.W. *Cantera, Version 2.6.0: An Object-oriented Software Toolkit for Chemical Kinetics, Thermodynamics, and Transport Processes*; Zenodo: Geneva, Switzerland, 2022. [CrossRef]
31. Shen, H.P.S.; Steinberg, J.; Vanderover, J.; Oehlschlaeger, M.A. A shock tube study of the ignition of n-heptane, n-decane, n-dodecane, and n-tetradecane at elevated pressures. *Energy Fuels* **2009**, *23*, 2482–2489. [CrossRef]
32. Ciezki, H.K.; Adomeit, G. Shock-tube investigation of self-ignition of n-heptane-air mixtures under engine relevant conditions. *Combust. Flame* **1993**, *93*, 421–433. [CrossRef]
33. Shu, B.; Vallabhuni, S.K.; He, X.; Issayev, G.; Moshammer, K.; Farooq, A.; Fernandes, R.X. A shock tube and modeling study on the autoignition properties of ammonia at intermediate temperatures. *Proc. Combust. Inst.* **2019**, *37*, 205–211. [CrossRef]
34. Wärtsilä Corporation. *Wärtsilä Encyclopedia of Ship Technology*, 2nd ed.; Wärtsilä Corporation: Helsinki, Finland, 2015; Volume 538. Available online: www.shippingencyclopedia.com (accessed on 17 February 2024).